Effects of Molecular Charge and Methyl Substitution on Proton Transfer between Oxygen Atoms

Eric A. Hillenbrand and Steve Scheiner*†

Contribution from the Department of Chemistry and Biochemistry, Southern Illinois University, Carbondale, Illinois 62901. *Received February 21, 1984*

Abstract: Proton transfers in $(HO-H-OH)^-$, $(H_2O-H-OH_2)^+$, and $(CH_3OH-H-HOCH_3)^+$ are compared via ab initio molecular orbital calculations by using a 4-31G basis set. In all three systems, lengthening the interoxygen H bond length leads to increases in the energy barrier to proton transfer. In the range of bond lengths studied, up to 2.95 Å, the barrier heights for $(H_2O-H-OH_2)^+$ and $(HO-H-OH)^-$ are quite similar while the barriers in $(CH_3OH-H-HOCH_3)^+$ are somewhat higher. These observations are explained on the basis of equilibrium OH bond lengths in the protonated subsystems and spatial extent of electron-density clouds. Angular deformations of the H bonds generally lead to enlargements of the transfer barriers. These enlargements are qualitatively similar for the two cationic systems whereas the anion behaves quite differently. It is shown that considerations of electrostatic interactions may account for the disparities between the two types of systems in a straightforward manner. Examination of the electron-density rearrangements that accompany the proton transfer lead to insights into the effects of overall charge and methyl substitution upon the process. The polarizability of the methyl group facilitates large contributions to the local shifts of density within the system while the negative charge of OH^- permits a greater net transfer of density from the proton-accepting molecule across the H bond to the donor.

Because of their widespread importance in a large number of chemical and biological processes, proton transfers have been subject to a great deal of recent investigation.[1-17] Work in this laboratory[18-23] has centered about study of proton transfers by ab initio molecular orbital methods in order to extract the fundamental features of this process. The prototype system used to examine proton transfers between oxygen atoms has been $(H_2OHOH_2)^+$ where the proton is exchanged between two equivalent water molecules. Comparison of the calculated data for this system with those containing nitrogen atoms has led to an understanding of the fundamental differences between O and N with regard to proton transfer. The energetics of proton exchange have been calculated for various configurations of the H bonds involving stretches and bends; moreover, analyses of the electronic redistributions accompanying the transfer have yielded insights into the interdependence of proton and electronic arrangements.

In addition to the distinctions between proton transfers involving different atoms, it is of interest also to determine how less drastic alterations of each system affect the proton transfer properties. Specifically, while the above $(H_2OHOH_2)^+$ system involves proton exchange between neutral waters, the transfer between negatively charged OH^- units in $(HO-H-OH)^-$ would provide an enlightening contrast; both systems are symmetric and involve oxygen atoms. Since the only difference is in the protonation states of the two groups involved in the transfer, the comparison is expected to provide some information about pH effects (taking into account, of course, that the calculations do not refer to a system fully exposed to solvent in a statistically averaged manner). In both the cationic $(H_2OHOH_2)^+$ and anionic $(HOHOH)^-$ systems, the oxygen atoms are bonded to hydrogen only. In order to obtain information on substituent effects, one hydrogen of each water of $(H_2OHOH_2)^+$ may be replaced by a methyl group. Thus, in $[(CH_3)HO-H-OH(CH_3)]^+$ the proton is exchanged between methanol molecules rather than waters. In this paper we report calculations of proton transfers in the $(HOHOH)^-$ and $(CH_3OH)_2H^+$ systems, and the data obtained are compared to previous results for $(H_2OHOH_2)^+$.

Methods and Results

All calculations were carried out at the restricted Hartree–Fock level by using a 4-31G basis set.[24] This split-valence set was chosen primarily to guarantee valid comparison with the previous data[18] for $(H_2OHOH_2)^+$ where this same basis was used. Despite the lack of polarization functions, this basis set has been demonstrated[18-23] to provide energetics of proton transfer that are in excellent agreement with much more time-consuming procedures

Table I. Optimized C_s Geometries of $(O_2H_3)^-$ and $(CH_3OH)_2H^+$ (see Figure 1). Also Included Is the C_{2v} Structure of $(O_2H_5)^+$ (from ref 18)

bond length, Å		bond angle, deg	
		$(O_2H_3)^-$	
O^a-O^b	2.457	$H^aO^aH^c$	108.8
O^a-H^c	1.102	$H^bO^bH^c$	108.7
O^a-H^a	0.955		
O^b-H^b	0.962		
	E^{SCF} = −151.20344 au		
		$(O_2H_5)^+$	
O^a-O^b	2.360	$H^aO^aH^c$	122.5
O^a-H^c	1.180	$H^bO^bH^c$	122.5
O^a-H^a	0.950		
O^b-H^b	0.950		
	E^{SCF} = −152.17703 au		
		$(CH_3OH)_2H^+$	
O^a-O^b	2.372	$H^aO^aH^c$	120.2
O^a-H^c	1.176	$H^bO^bH^c$	120.4
O^a-H^a	0.952	$C^aO^aH^c$	123.6
O^b-H^b	0.952	$C^bO^bH^c$	123.7
O^a-C^a	1.476	$H^a{}_1C^aO^a$	106.0
O^b-C^b	1.474	$H^a{}_2C^aO^a$	108.4
$C^a-H^a{}_1$	1.074	$H^b{}_1C^bO^b$	106.0
$C^a-H^a{}_2$	1.075	$H^b{}_2C^bO^b$	108.5
$C^b-H^b{}_1$	1.074	$\phi(H^a{}_2C^aO^aH^a)$	60.9
$C^b-H^b{}_2$	1.075	$\phi(H^b{}_2C^bO^bH^b)$	60.9
	E^{SCF} = −230.12218 au		

† Recipient of an NIH Research Career Development Award, 1982–1987.

(1) E. Caldin and V. Gold, Eds., "Proton Transfer Reactions", Chapman and Hall, London, 1975; "Electron and Proton Transfer", *Faraday Discuss. Chem. Soc.*, **No. 74**, (1982); M. Meot-ner, In "Gas Phase Ion Chemistry", M. T. Bowers, Ed., Academic, New York, Vol. 1, 1979, pp 187–271; M. Meot-ner, *J. Am. Chem. Soc.*, **104**, 5 (1982).
(2) P. Ausloos and S. G. Lias, *J. Am. Chem. Soc.*, **103**, 3641 (1981).
(3) R. R. Squires, V. M. Bierbaum, J. J. Grabowski, and C. H. DePuy, *J. Am. Chem. Soc.*, **105**, 5185 (1983).
(4) K.-Å. Engdahl, H. Bivehed, P. Ahlberg, and W. H. Saunders, Jr., *J. Am. Chem. Soc.*, **105**, 4767 (1983).
(5) L. Schriver, A. Schriver, and J. P. Perchard, *J. Am. Chem. Soc.*, **105**, 3843 (1983).
(6) W. E. Farneth and J. I. Brauman, *J. Am. Chem. Soc.*, **98**, 7891 (1976); J. M. Jasinski and J. I. Brauman, *Ibid.*, **102**, 2906 (1980).
(7) F. M. Menger, J. F. Chow, H. Kaiserman, and P. C. Vasquez, *J. Am. Chem. Soc.*, **105**, 4996 (1983); F. M. Menger, *Tetrahedron*, **39**, 1013 (1983).
(8) R. W. Alder, R. E. Moss, and R. B. Sessions, *J. Chem. Soc.*, 997, 999, 1000 (1983).

0002-7863/84/1506-6266$01.50/0

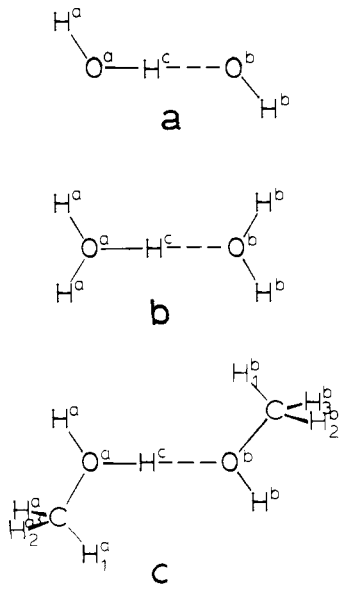

Figure 1. Geometries of complexes and atomic labeling schemes.

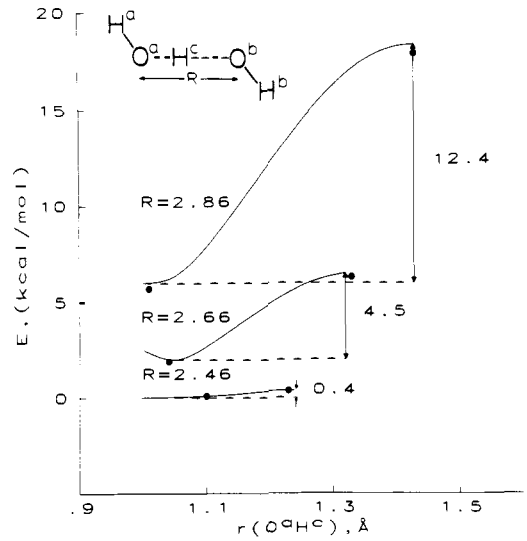

Figure 2. Calculated proton transfer potentials and energy barriers for $(O_2H_3)^-$. Each curve is labeled with the interoxygen distance R. Filled circles indicate energies of geometries fully optimized under constraint of R value shown. All energies are shown relative to that of the fully optimized structure with R = 2.46 Å and r = 1.10 Å.

including large polarized basis sets and electron-correlation effects. The calculations were carried out by using the GAUSSIAN-80 package of computer programs developed by Pople and coworkers.[25]

I. **Linear H Bonds.** As a first step, geometry optimizations of both the $(HOHOH)^-$ and $(CH_3OH)_2H^+$ systems were carried out subject to the following restrictions. $(HOHOH)^-$ was held in a planar C_s configuration with the two terminal hydrogens trans to one another. Also, the central hydrogen was assumed to lie along the O--O internuclear axis. Previous calculations have placed similar constraints on this system,[17,23] and in fact, recent calculations by Rohlfing et al.[16] have provided evidence that deviations from these restrictions in the fully optimized geometry are quite small. A full geometry optimization of $(CH_3OH)_2H^+$ was carried out here and led also to a C_s structure with a linear O—H--O bond. The geometries of these two complexes are illustrated in Figure 1 along with the structure of $(H_2O)_2H^+$ and the optimized geometrical parameters summarized in Table I.

One notable feature of the geometries reported in Table I is the shortness of the intermolecular distances. The R(OO) H bond lengths are 2.46 and 2.37 Å for the $(O_2H_3)^-$ and $(CH_3OH)_2H^+$ systems, respectively. These short bonds are not surprising in light of the strong nature of the bond in these charged complexes. For example, the calculated energy of dissociation of the methanol dimer complex to CH_3OH and $CH_3OH_2^+$ is 38.0 kcal/mol, much greater than that for typical uncharged complexes.

Perhaps more important is the fact that in the H bonds of $(O_2H_3)^-$ and $(CH_3OH)_2H^+$ the central proton H^c does not lie at the midpoint of the O^a--O^b axis. This fact indicates that the potential for proton transfer in these systems will contain a pair of equivalent equilibrium minima (O—H--O and O--H—O) with an energy barrier separating them. The asymmetries of the H bonds are not large; for example, H^c lies only 0.01 Å from the O--O midpoint in the methanol dimer. Thus, the two minima may be expected to lie rather close to one another, and the energy barrier at the transfer midpoint should be quite low.

This prediction is in fact borne out by calculation of the energetics involved in the transfer of the proton between O^a and O^b. The lowest curve in Figure 2 illustrates the energetics of proton transfer in $(O_2H_3)^-$ at its equilibrium H-bond length of 2.46 Å. It may be seen that motion of H^c from its equilibrium position 1.10 Å from O^a to the midpoint of the O--O axis leads to an increase in energy of only 0.4 kcal/mol. For the methanol dimer, the proton transfer potential associated with the equilibrium H-bond length of 2.37 Å is even shallower than this, being essentially flat. The other curves in Figure 2 represent energetics of proton transfer in $(H_3O_2)^-$ for R(OO) distances longer than the equilibrium value. (Each curve corresponds to the left half of the full symmetric transfer potential.) It is clear that as the two oxygen atoms are further separated from one another, the energy barrier that the proton must surmount in order to transfer from O^a to O^b increases.

The energetics in Figure 2 were calculated by using the "rigid molecule" approximation[18-20] wherein all nuclei are held fixed in the geometry specified in Table I as the proton is allowed to move between the two oxygens. In order to check the validity of this approximation, full geometry optimizations were carried out for both the minimum and maximum of each curve in Figure 2. The energies of the optimized structures are indicated by the filled circles from which it may be seen that the optimizations lead to only very small changes in the total energies of each point. Moreover, the stabilizations of the minima and maxima of each

(9) R. Rossetti, R. Rayford, R. C. Haddon, and L. E. Brus, *J. Am. Chem. Soc.*, **103**, 4303 (1981).
(10) B. H. Meier, F. Graf, and R. R. Ernst, *J. Chem. Phys.*, **76**, 767 (1982).
(11) E. Grunwald, *J. Phys. Chem.*, **86**, 1302 (1982).
(12) S. Nagaoka, T. Terao, F. Imashiro, A. Saika, N. Hirota, and S. Hayashi, *J. Chem. Phys.*, **79**, 4694 (1983); *Chem. Phys. Lett.*, **80**, 580 (1981); S. Nagaoka, N. Hirota, T. Matsushita, and K. Nishimoto, *Ibid.*, **92**, 498 (1982).
(13) K. Sato, S. Tomoda, K. Kimura, and S. Iwata, *Chem. Phys. Lett.*, **95**, 579 (1983); S. Tomoda and K. Kimura, *Chem. Phys.*, **74**, 121 (1983).
(14) H. Z. Cao, M. Allavena, O. Tapia, and E. M. Evleth, *Chem. Phys. Lett.*, **96**, 458 (1983).
(15) M. D. Newton, *J. Chem. Phys.*, **67**, 5535 (1977); J. H. Busch and J. R. de la Vega, *J. Am. Chem. Soc.*, **99**, 2397 (1977).
(16) C. M. Rohlfing, L. C. Allen, C. M. Cook, and H. B. Schlegel, *J. Chem. Phys.*, **78**, 2498 (1983).
(17) B. O. Roos, W. P. Kraemer, and G. H. F. Diercksen, *Theor. Chim. Acta*, **42**, 77 (1976); A. Stogard, A. Strich, J. Almlöf, and B. Roos, *Chem. Phys.*, **8**, 405 (1975); G. Karlström, B. Jönsson, B. Roos, and H. Wennerström, *J. Am. Chem. Soc.*, **98**, 6851 (1976).
(18) S. Scheiner, *J. Am. Chem. Soc.*, **103**, 315 (1981); *Ann. N.Y. Acad. Sci.*, **367**, 493 (1981).
(19) S. Scheiner, *J. Phys. Chem.*, **86**, 376 (1982).
(20) S. Scheiner, *J. Chem. Phys.*, **77**, 4039 (1982); **80**, 1982 (1984).
(21) S. Scheiner and L. B. Harding, *J. Am. Chem. Soc.*, **103**, 2169 (1981); *Chem. Phys. Lett.*, **79**, 39 (1981); *J. Phys. Chem.*, **87**, 1145 (1983).
(22) S. Scheiner, *J. Chem. Phys.*, **75**, 5791 (1981).
(23) (a) M. M. Szczesniak and S. Scheiner, *J. Chem. Phys.*, **77**, 4586 (1982). (b) S. Scheiner, M. M. Szczesniak, and L. D. Bigham, *Int. J. Quantum Chem.*, **23**, 739 (1983).
(24) R. Ditchfield, W. J. Hehre, and J. A. Pople, *J. Chem. Phys.*, **54**, 724 (1971).
(25) J. S. Binkley, R. A. Whiteside, R. Krishnan, R. Seeger, D. J. DeFrees, H. B. Schlegel, S. Topiol, L. R. Kahn, and J. A. Pople, *QCPE*, No. **406** (1981).

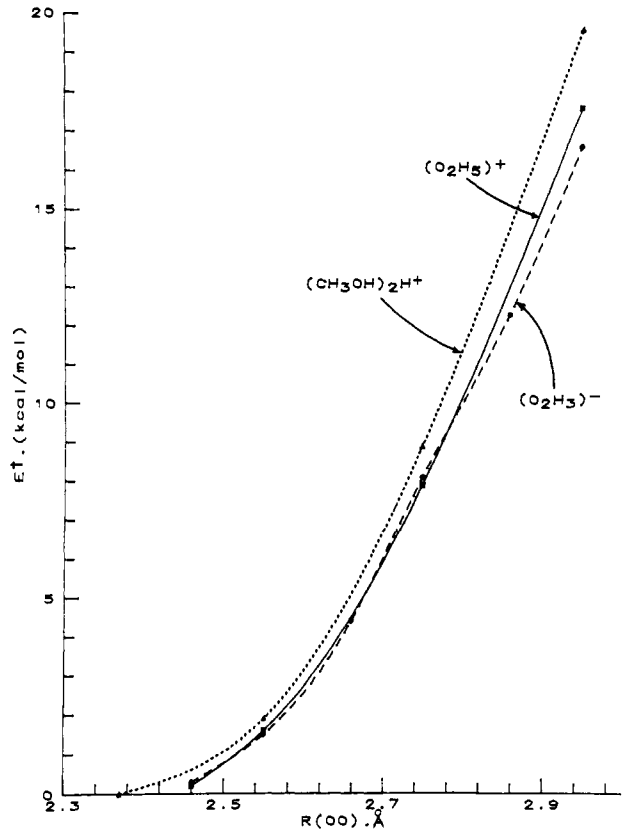

Figure 3. Calculated proton transfer energy barriers as a function of the interoxygen separation.

curve are nearly identical, leading to the conclusion that the energetics of proton transfer calculated with the rigid molecule approximation and with full geometry optimizations are essentially identical. The validity of the rigid molecule approximation was verified also in the $(CH_3OH)_2H^+$ system by comparison with optimized geometries. In fact, the largest deviation between optimized and rigid molecule proton transfer barriers in either system was only 2%.

A detailed comparison between the energetics of proton transfer in the anionic $(HOHOH)^-$ and two cationic $(H_2OHOH_2)^+$ and $(CH_3OH)_2H^+$ systems is presented in Figure 3. Each curve illustrates the dependence of the proton transfer barrier, $E^\dagger$, defined as the difference in energy between the maximum and minimum of each transfer potential, upon the interoxygen distance. In general, the barriers of all three systems are fairly similar to one another. However, as the $R(OO)$ distance increases, the barrier in the methyl-substituted $(CH_3OH)_2H^+$ system increases more quickly than that for the other two cases. The total molecular charge seems to have little effect on the barrier height as the $(H_2OHOH_2)^+$ and $(HOHOH)^-$ curves lie quite close to one another throughout the range studied which goes up to 2.95 Å.

The near coincidence of the transfer barriers for $(H_2OHOH_2)^+$ and $(HOHOH)^-$ is somewhat surprising in light of the different charges of the two systems. However, this fact does not appear to be an artifact of the SCF/4-31G procedure being used here. This technique has been shown capable of reproducing quite well the energetics of proton transfer calculated with extended basis sets and including consideration of electron correlation via a large number of configurations in the CI list.[18-23] When a polarized triple-valence basis set was used in conjunction with third-order Moller–Plesset perturbation theory, the energy barriers in $(H_2OHOH_2)^+$ and $(HOHOH)^-$, both with $R(OO) = 2.74$ Å, were found to be equal.[23b] Basis set superposition does not introduce any appreciable errors into our results either, as demonstrated by calculations with the counterpoise procedure.[23a] The near absence of an effect of molecular charge upon the transfer barriers for H-bond lengths in this range does therefore seem to be verified by higher levels of theory.

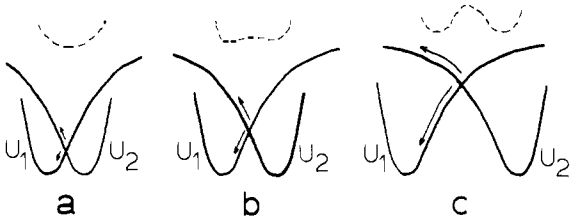

Figure 4. Idealized proton-dissociation curves. Arrows represent changes in energy resulting from motion of the proton away from the midpoint of the H bond. The shortest H-bond length is represented by point a; c contains the longest bond. Dashed curves indicate the sum of two potentials, $U_1 + U_2$.

Source of Comparative Energetics. It is of some fundamental interest to understand the reasons underlying the comparative proton transfer barrier heights in the three systems. The simplest point to explain is the rise in barrier height with increased interoxygen separation in all three systems. The barrier is defined as the difference in energy between the midpoint and starting-point configurations. At the starting point, the system may be described as containing a covalent O–H bond and a weaker H--O interaction. When the proton has reached the midpoint, the covalent bond has weakened while the second interaction has become stronger. The higher total energy of the midpoint arises from the fact that the stabilization of the second interaction cannot compensate for the partial breaking of the covalent bond. As the distance between the two oxygen atoms is increased, the proton must move further to reach the midpoint and the covalent bond is consequently weakened that much more, leading to a higher transfer barrier. The extreme case would be that of infinite separation where the proton would need to become fully dissociated from the first molecule before it could approach the second. In such a case, the proton transfer barrier would be identical with the proton affinity of the molecule concerned.

An oversimplified but nonetheless instructive manner of describing the energetics of proton transfer is by way of proton dissociation curves for each molecule. As shown in Figure 4, the curves are oriented in opposite directions to account for the fact that proton transfer involves simultaneous dissociation of the proton from one molecule and association with the other. As a first approximation to the total energy of the system we take the sum of the two curves U_1 and U_2, shown as a dashed curve above each pair. In all cases, the two curves intersect at the midpoint of the transfer. We will focus our attention on the behavior of the total energy as the proton moves away from this central point and toward one of the O atoms. Figure 4a represents a relatively small interoxygen separation, R, and the curves are hence rather close together. As the proton moves to the left, the energies of the two curves follow the arrows as indicated. If we assume that the shapes of the curves are approximately parabolic near their minima, the energy increase associated with U_2 is greater than the decrease of U_1; hence the total energy of the system increases as the proton moves from the midpoint, and a single-minimum symmetric potential is expected. If R is increased somewhat, as is the case in Figure 4b, the crossing point occurs higher up on each curve. If we assume that the general characteristics of the dissociation curves are not unlike the standard Morse-type functions, the crossing point might occur above the point of inflection of each curve. Consequently, the increase in U_2 would be smaller than the decrease associated with U_1, and motion of the proton away from the midpoint leads to an overall stabilization. The symmetric potential therefore must contain two minima with an energy barrier separating them. Further increase in interoxygen distance leads to the situation depicted in Figure 4c where the stabilization of U_1 is much greater than the energy increase of U_2. Thus, the energy difference between the midpoint and starting-point configurations, or $E^\dagger$, has increased substantially.

Evaluation of the energy barriers by addition of the individual proton-dissociation curves, each calculated by HF/4-31G, was found to lead to proper behavior. All energy barriers increased uniformly as the intermolecular distance was lengthened. Of

Table II. Mulliken Population Changes Associated with Half-Proton Transfer[a]

	$(O_2H_3)^-$	$(O_2H_5)^+$	$(CH_3OH)_2H^+$	$(O_2H_3)^-$	$(O_2H_5)^+$	$(CH_3OH)_2H^+$
Δr, Å	0.337	0.349	0.386	0.279	0.279	0.279
groups						
$(HOX)^a$	112	120	141	91	91	106
$(HOX)^b$	−112	−91	−105	−96	−77	−70
atoms						
H^c	0	−29	−37	5	−14	−36
O^a	66	48	36	51	30	37
O^b	−58	−12	14	−49	−11	11
H^a	46	36	39	40	30	26
H^b	−54	−40	−43	−47	−33	−29
X^a		36	66		30	43
X^b		−40	−76		−33	−53
orbitals (O^a)						
2s	21	23	32	14	15	27
$2p_z$	96	79	82	80	59	64
$2p_x$	−51	−55	−74	−44	−45	−51
$2p_y$	0	0	−4	0	0	−2
orbitals (O^b)						
2s	−8	−15	−16	−7	−12	−12
$2p_z$	−102	−51	−44	−87	−44	−28
$2p_x$	51	54	70	44	45	48
$2p_y$	0	0	4	0	0	3

[a] All entries in millielectrons; positive values refer to an increase in density. a and b superscripts refer to proton-donating and -accepting molecules, respectively; H^c is the central proton being transferred. The p_z orbitals point along the H-bond axis and p_x lie in the molecular plane. The X-atom designation refers to H for $(O_2H_5)^+$, to (CH_3) for $(CH_3OH)_2H^+$, and is absent in $(O_2H_3)^-$.

course simple summation of the energies associated with U_1 and U_2 is only partially valid as it neglects the effect of the presence of one molecule upon the proton dissociation properties of the other. For the midpoint configuration A--H--A′, these interactions include the equivalent effects of A′ upon A--H and A upon H--A′. For the starting point, A-H--A′, the effect of A′ upon A–H is expected to be much smaller than the effect of A upon H---A′. In fact, the close proximity of A to H in this configuration would certainly make the latter component the largest perturbation on the isolated proton dissociations. Treating this component as dominant, the molecular interactions would preferentially stabilize the end-point configuration leading to an increase in the transfer barrier. This is indeed found to be the case as the transfer barriers computed by using the full systems are uniformly higher than those calculated by the summation of proton dissociations outlined above.

We therefore now have at our disposal a useful means of analyzing the underlying reasons for the difference in proton transfer barriers observed in Figure 3. First of all, one would expect the shapes of the proton dissociation potentials for water and methanol to be quite similar, particularly near the minima. The proton affinities of these two molecules, calculated with the 4-31G basis set, are fairly close at 183 and 200 kcal/mol, respectively. However, geometry optimizations of the two protonated molecules reveal that the equilibrium r(OH) bond length is 0.005 Å shorter for $CH_3OH_2^+$ than for OH_3^+. The shortening of this distance is equivalent to translating the U_1 curve to the left by this amount and U_2 to the right, which has an effect identical with that of lengthening the interoxygen separation R by 0.01 Å. It is therefore not surprising that the energy barriers in the protonated methanol dimer are slightly greater than those for $(H_2O)_2H^+$. It is of particular interest that a displacement of the $(CH_3OH)_2H^+$ curve to the right by about 0.01 Å in Figure 3 would place it in near coincidence with the water dimer curve, particularly for small values of R. A last point to be made in this regard is that the difference in equilibrium bond lengths between OH_3^+ and NH_4^+ is 0.05 Å at the 4-31G level and that it has been pointed out previously[19] that the curve of proton transfer barriers for $(H_2O)_2H^+$ in Figure 3, shifted to the right by twice this amount, would lie very close to the analogous curve for $(H_3N)_2H^+$.

The equilibrium bond length in H_2O is 0.013 Å shorter than that in H_3O^+. Using the same reasoning as above, one would expect the transfer barriers in $(OH)^-_2H^+$ to be significantly higher than those in $(H_2O)_2H^+$. Moreover, the proton dissociation curve for OH^- should be considerably steeper than that of OH_2 since its 4-31G proton affinity is more than twice that of water. The steeper U_1 and U_2 curves would be a second factor leading to a higher proton transfer barrier. However, as noted above, for R(OO) distances of less than 3 Å this is not the case, the transfer barriers being nearly identical. These results are not surprising if one keeps in mind that the proton is being transferred between OH^- anions in one case and between neutral water molecules in the other. The electrons in the anion are more available for bonding to the proton; the electron density is greater in the direction of the approaching proton, as determined by 4-31G calculations. In other words, the contours of isoelectron density reach out further from the oxygen nucleus in the case of the anion. Thus, while the proton dissociation curve may be steeper for OH^-, there would be a tendency for the inflection point to occur at a longer O--H distance. Comparison of the 4-31G proton dissociation curves confirms these predictions. The nearly equal proton transfer barriers for $(H_2O)_2H^+$ and $(OH)^-_2H^+$ therefore appear to result from the cancellation between two opposing effects: the greater proton affinity of OH^- and its more spatially extended electron distribution.

Electron-Density Rearrangements. The electronic structures provide a rich source of information about the fundamental characteristics of proton transfers between oxygen atoms in the different bonding situations studied here. The redistributions of electron density that accompany half-proton transfer are displayed in the form of contour maps in Figure 5. The contours represent the change in total electron density resulting from motion of the proton from its equilibrium position near the left-hand or proton-donating oxygen atom O^a (tail of the arrow) to the midpoint of the O--O axis (arrowhead). Increases in density are indicated by solid contours and decreases by dashed lines. The contours are labeled in a negative logarithmic fashion such that greater density changes are represented by smaller numerical labels. The region chosen for display as containing the most information is the xz plane which contains all atoms of the $(O_2H_3)^-$ and $(O_2H_5)^+$ systems and all but 2 hydrogens of each methyl group of $(CH_3OH)_2H^+$.

An alternate manner of studying the electronic distributions is by use of Mulliken population analyses. Table II contains the changes in population as a result of half-proton transfer for each of the three systems in Figure 5. The data are arranged first by groups, e.g., proton-donor or -acceptor molecule, then by individual atoms, and finally by atomic orbitals on each oxygen. Positive entries refer to density increase and negative to loss. The data in the first three columns of Table II and the corresponding three plots in Figure 5 may be used in complementary fashion since they

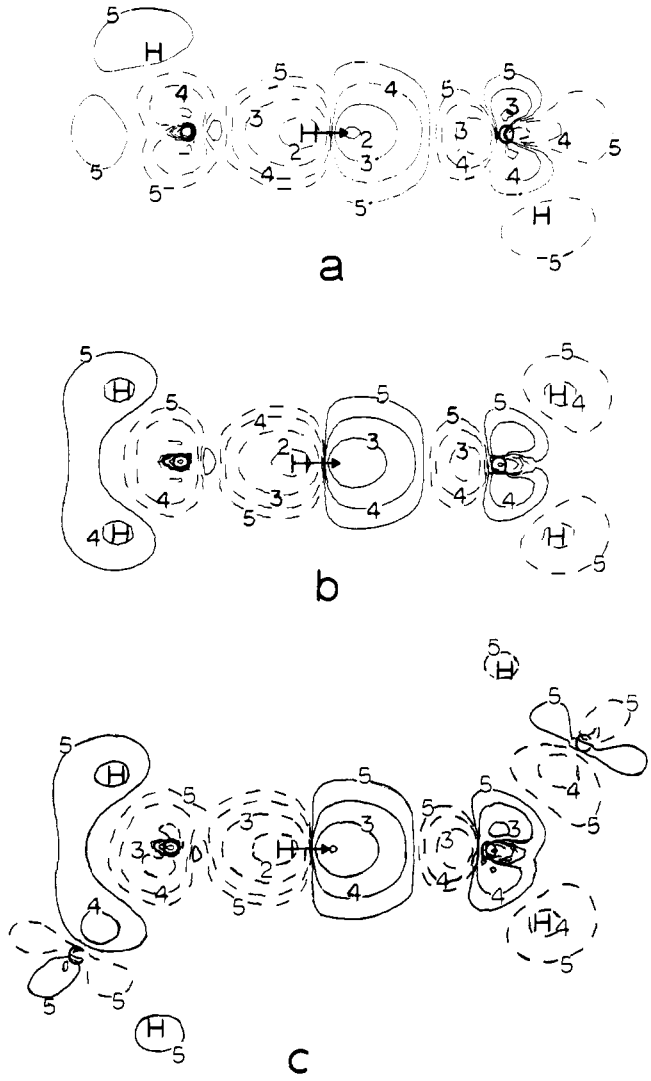

Figure 5. Electron-density difference maps for (a) $(O_2H_3)^-$, (b) $(O_2H_5)^+$, and (c) $(CH_3OH)_2H^+$. Contours represent difference in density between configuration with the proton at the midpoint of the bond and that with the proton at the starting point (O—H--O). Solid contours indicate gain and dashed contours decrease in density. Numerical labels are equal to the negative of twice the log of the density change (in e/au^3). All atoms are included in the plane shown except two hydrogens from each methyl group in part c.

pertain to identical proton half-transfers.

There are a number of features common to all three systems and which are presumably general to proton transfers involving oxygen atoms. The most obvious is the charge loss and gain respectively about the tail and head of the arrow, caused simply by the motion of the proton and its accompanying electron cloud. Also present is a domain of density depletion in the lone-pair region to the left of the proton-accepting O^b; the corresponding increase immediately to the right of O^a is much less prominent, represented by a single contour line encompassing a small area. The atoms of the proton-accepting groups are surrounded by regions of charge loss indicating an overall decrease in density, confirmed by the negative entries for $(HOX)^b$ in Table II. This density loss is generally shared to some extent by all atoms in the molecule via a mechanism involving polarization of the internal OH and OC bonds. This polarization is evidenced by the pattern of dashed and solid contours located between the H (or C) and O nuclei in Figure 5 as well as the density reductions on H^b and increase in population observed in the $2p_x$ orbital of the O^b atom. Very analogous patterns, but in the opposite sense, may be noted for the $(HOX)^a$ molecule.

In addition to the features that are common to interoxygen proton transfers, we are interested particularly in those properties that distinguish one system from another so as to elucidate the effects of overall charge and methyl substitution upon the process. For example, the first row of electronic data in Table II indicates that the proton-donating methanol molecule acquires more density (141 me) as a result of half-proton transfer than do OH_2 or OH^-. The sink for this excess charge is neither O^a nor H^a but rather the methyl group X^a. The lower left corner of Figure 5c illustrates the spatial distribution of the additional methyl density. The solid contours indicate charge accumulation on the H atoms as well as on C. The dashed lobes flanking the carbon suggest that the density shift to the hydrogens occurs via polarization of the appropriate CH bonds. Similar observations apply to the methyl group of the proton-accepting molecule although the signs of density changes are reversed. It is therefore concluded that the methyl group serves an important function as source or sink of electron density during proton transfers. The charge is transmitted by polarization of CH and CO bonds.

Although the geometries of all three systems in Figure 5 were constructed such that $R(OO) = 2.75$ Å, the slightly different equilibrium O–H bond lengths lead to inequalities in the distances of motion of the central proton to the midpoint of the O--O axis. It is possible that these different distances, contained at the top of Table II as Δr, may result in an imbalance of the data contained therein. To ensure consistency, a second set of data was generated in which all three protons move an identical distance, 0.279 Å; the associated population changes are listed in the last three columns of Table II. These data verify that the conclusions stated above about the charge shifts involving the methyl groups are indeed valid and not an artifact of the specific proton transfer distance.

We turn our attention now to the proton-accepting groups which Table II shows to suffer overall depletions of density during the proton transfer process. The numerical data indicate that it is the OH^- unit of $(O_2H_3)^-$ which loses substantially more charge than either of the neutral OH_2 or CH_3OH molecules of the other two systems. This greater charge loss is probably associated with the more polarizable character of the OH^- anion. The atomic population changes associate the greater density loss with both the H and O atoms. It is possible to further pinpoint the large density depletion of the O^b atom of $(O_2H_3)^-$ as arising from the $2p_z$ orbital where this atom loses 102 me, as compared to 51 and 44 for the cationic systems. The involvement of this orbital is clearly indicated also by the extensive dashed contours to the right of O^b in Figure 5a, contours which are nearly absent in Figure 5, parts b and c.

Another interesting point concerning the proton-accepting O^b atoms is the fact that the density change of this oxygen is positive for $(CH_3OH)_2H^+$ whereas it is negative for the other two systems. The charge pickup by the O^b atom may be attributed largely to the previously described ability of the methyl group to donate its charge to the oxygen via polarization of the CO and CH bonds.

It is worthy of note that despite the variance in the population changes of the oxygen atoms from one system to another, the contours in the lone-pair regions are remarkably constant. In all cases, a single small "5" contour is present to the right of O^a and a set of three dashed contours appear to the left of O^b. These similarities may be directly related to the nearly equal energy barriers to proton transfer reported in the previous section.

A final point concerns the central proton H^c. Table II indicates that in both cationic systems, this proton loses density as it shifts from its equilibrium position to the O--O midpoint. However, in the anionic $(O_2H_3)^-$ system, the change is minimal or slightly positive. This fact is reflected in the generally larger size of the "2" and "5" solid contours about the arrowhead in Figure 5a. The reason for this distinction is probably related to the larger size of the O lone pairs in the anionic OH^- units.

II. Angular Deformations of H Bond. The calculations described up to this point have dealt only with geometries in which the orientations of the proton-donating and -accepting molecules have been optimized relative to one another. The electronic densities associated with these geometries are such that the most energetically favorable position of the central proton during the

Table III. Increases of Proton Transfer Barrier, $\Delta E^{\dagger}$, and Distortion Energies for Starting Points (OH--O) and Midpoints (O--H--O) of Proton Transfer (All Entries in kcal/mol; R(OO) = 2.75 Å in All Cases)

	$\Delta E^{\dagger}$		ΔE(OH--O)		ΔE(O--H--O)	
(α_a,α_b)	$(O_2H_5)^+$	$(O_2H_3)^-$	$(O_2H_5)^+$	$(O_2H_3)^-$	$(O_2H_5)^+$	$(O_2H_3)^-$
(40,0)	6.1	−2.8	9.2	13.2	15.3	10.4
(0,−40)	5.0	6.1	10.3	4.3	15.3	10.4
(40,40)	10.9	1.8	14.5	12.7	25.4	14.5
(−40,−40)	10.9	8.3	14.5	6.2	25.4	14.5
(40,−40)	17.5	3.6	21.2	18.8	38.7	22.4

entire course of its transfer lies directly along the O--O axis and a "linear" H-bond results. However, there are a great many H bonds that occur in chemical and biological systems where restraints imposed by the overall molecular structure prevent adoption of a linear arrangement of each H bond.[7-9,26] It is therefore of great importance to address the question of the effects of angular distortions of the H bond upon the proton transfer properties.

To this end, angular deformations were imposed on the H bonds of the three systems as follows. Starting with the optimized geometries described in Figure 1, a pair of vectors is associated with each system. $\mathbf{v}_a$ originates on the left-hand proton-donating oxygen atom O^a and points directly toward O^b; $\mathbf{v}_b$ points from O^b toward O^a. The entire left-hand molecule, including $\mathbf{v}_a$, is then rotated in a counterclockwise direction by an amount α_a such that $\mathbf{v}_a$ is directed above the O--O axis by α_a. An analogous rotation of the right-hand molecule so that $\mathbf{v}_b$ points above the O--O axis is designated as α_b (note that the associated rotation of the right-hand molecule is clockwise). In either case, negative values of α_a or α_b correspond respectively to rotations of $\mathbf{v}_a$ or $\mathbf{v}_b$ below the O--O axis. These deformations may alternately be described as rotations of each molecule about a line passing through O^a or O^b and perpendicular to the plane of the paper in Figure 1.

For each of several configurations of the H bond, specified by the interoxygen distance R and the pair of angles α_a and α_b, potentials for proton transfer were computed, holding all atoms fixed in place except the central proton which was allowed to follow the lowest energy path between the two oxygens. These potentials were calculated for the $(O_2H_3)^-$ system for three different interoxygen separations varying between 2.55 and 2.95 Å. For each value of R, a number of different types of angular distortions were examined. The first mode has the proton-donating molecule rotated upward (counterclockwise) but leaves the other molecule unchanged. If we denote this mode in terms of the pair of (α_a,α_b) angles, it would be written as $(\alpha,0)$. In the second mode, the notation is $(0,-\alpha)$ as the first molecule is left unrotated but the proton-accepting molecule is rotated downward. Both molecules are rotated in the remaining three modes; both upward by equal amounts in mode 3 (α,α) and both downward in 4 $(-\alpha,-\alpha)$. The last mode rotates the two molecules in opposite directions $(\alpha,-\alpha)$.

The energy barriers computed for proton transfer in the $(O_2H_3)^-$ system are presented in graphical fashion as a function of the angle α in Figure 6. The effects of the H-bond deformations upon the energetics of transfer vary a great deal from one bending mode to the next. For example, rotation of the proton-donating molecule upward results in a reduction in the transfer barrier while increases are produced by all four of the other modes. This increase is rather mild for mode 3 where both molecules rotate upward by equal amounts but is more dramatic for mode 2 (rotation of the proton acceptor) and for mode 4 where both molecules are rotated downward. The remaining mode (5), involving rotation of the two molecules in opposite directions, is intermediate between the mild and dramatic cases above.

Comparison between Cation and Anion. The effects of angular deformations upon the proton transfer energetics of the cationic $(O_2H_5)^+$ system have been reported previously[18] and exhibit somewhat different behavior than that illustrated for the anion

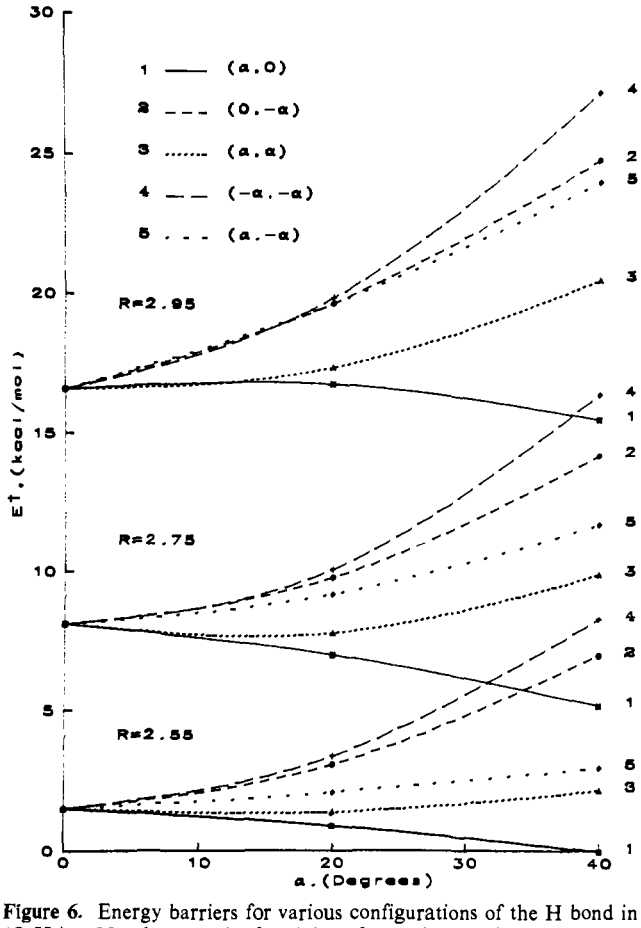

Figure 6. Energy barriers for various configurations of the H bond in $(O_2H_3)^-$. Numbers on the far right refer to the angular deformation mode.

in Figure 6. The increases in proton transfer barrier arising from 40° distortions of various types for R(OO) = 2.75 Å are presented under the heading of $\Delta E^{\dagger}$ in Table III and clearly illustrate the disparities between the two systems. As these proton transfer energy barriers represent the difference in energy between the starting points (OH--O) and midpoints (O--H--O) for each transfer, our analysis will focus upon the effects of angular deformations upon the energies of each of these configurations. The two columns of data in Table III under the heading of ΔE(OH--O) contain the energy increase associated with distorting the starting-point configurations of the $(O_2H_5)^+$ and $(O_2H_3)^-$ systems to the (α_a,α_b) angles indicated at the left, as compared to the (0,0) structure. The last two columns list the analogous quantities for the distorted vs. undistorted midpoint geometries. (The difference between distortion energies of the midpoint and starting point is equal to the change in barrier height $\Delta E^{\dagger}$.)

A first examination of the data in Table III reveals several overall features. In general, the energy barriers resulting from angular distortions are greater for the cationic than anionic system. The same pattern is noted in the distortion energies of the starting point and midpoint structures (with several important exceptions). There are also some surprising results such as the *decrease* in barrier height of 2.8 kcal resulting from rotation of the proton-donating molecule in $(O_2H_3)^-$. This same mode (α_b = 0) also

(26) C. Ceccarelli, G. A. Jeffrey, and R. Taylor, *J. Mol. Struct.*, **70**, 255 (1981); S. N. Vinogradov, In "Molecular Interactions", H. Ratajczak and W. J. Orville-Thomas, Eds., Wiley, New York, 1981, Vol. 2, pp 179–229.

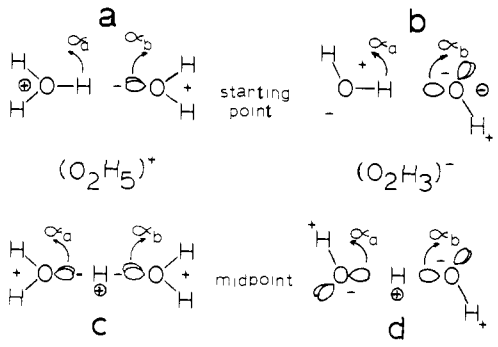

Figure 7. Starting-point and midpoint structures for proton transfers in $(O_2H_5)^+$ and $(O_2H_3)^-$. Positive or negative group charge is indicated by a circled + or − sign. Uncircled symbols designate positive and negative ends of dipole moments.

presents the case of a larger distortion energy of the starting point of $(O_2H_3)^-$ than of $(O_2H_5)^+$. The second line of data brings out an exception to the general rule stated above in that for the $\alpha_a = 0$ mode, the barrier increase is somewhat larger for the anion than for the cation.

As an aid in understanding the underlying reasons for the dependence of the barrier heights upon the various H-bond distortions, the structures of the starting-point and midpoint configurations of the two systems are illustrated schematically in Figure 7. The geometries shown are undistorted; the curved arrows indicate the direction of rotation of each molecular unit for positive values of α_a and α_b. A simplifying assumption of sp^3 hybridization of the O atoms is used to sketch the lone-pair orientations; however, the specific type of hybridization is not essential to the points to be discussed below. Our explanation of the magnitudes of the distortion energies will be based primarily upon two considerations. Energies are expected to increase as a result of misalignment of the O–H bond and the accepting lone pairs. An important distinction is therefore the fact that OH_2 contains two O lone pairs while three are present in OH^-. Our second argument is based on electrostatics in which we consider the charge distributions of each subunit. The near D_{3h} symmetry of the OH_3^+ segment of Figure 7a leads to a negligible dipole moment. OH_2 is uncharged with a dipole moment which points along the HOH bisector. The OH^- anion bears an overall negative charge and contains a buildup of negative charge opposite the H atom. The overall charges of OH_3^+ and OH^- are indicated in Figure 7 by the + and − symbols with the circles around them. The uncircled symbols represent the dipole moments of the OH_2 and OH^- species.

We begin our analysis with the distortion energies of the starting-point geometries, listed in the fourth and fifth columns of Table III. The counterclockwise rotation of the proton-donating molecule by 40° leads to energy increases of the $(O_2H_5)^+$ and $(O_2H_3)^-$ systems of 9.2 and 13.2 kcal/mol, respectively. These increases are understandable in light of the rotation of the O–H bond away from the lone pairs of the other molecule. The larger increase for the anionic system may be explained as follows. The main electrostatic contribution to the energy of the structure in Figure 7a is the interaction between the overall charge of OH_3^+ on the left and the dipole moment of neutral OH_2 on the right. Rotation of the left-hand OH_3^+ unit has little effect on this term; the direction of the OH_2 dipole moment is unchanged. On the other hand, counterclockwise rotation of the left-hand OH_2 unit in Figure 7b turns the positive end of the OH_2 dipole further away from the negatively charged OH^- on the right, resulting in an increase of energy. This effect is further augmented by consideration of the dipole of OH^-, the negative end of which is separated from the positive end of the OH_2 dipole by rotation of the latter. The situation is reversed when the right-hand unit is rotated counterclockwise (0,−40) and the distortion energy of the cation is substantially greater than that for the anion. In Figure 7b, the dipole of OH_2 is not rotated and its interaction with the negative charge of OH^- is consequently unchanged. The dipole of OH^- is brought into an orientation slightly more favorable for interaction with the OH_2 dipole. Whereas the electrostatic energy of the $(O_2H_3)^-$ anion is lowered somewhat by the (0,−40) rotation, that of the cation is greatly increased as a result of the rotation of the dipole of the right-hand OH_2 away from the OH_3^+ unit. Another point which may have some relevance is the number of lone pairs on the two proton-accepting molecules. Counterclockwise rotation of the OH^- species in Figure 7b brings the two out-of-plane lone pairs more in line with the central proton while the same may not be said for OH_2 in Figure 7a. It is therefore not unreasonable to expect a less drastic increase in energy in the case of the $(O_2H_3)^-$ system.

The third mode in Table III involves rotation of both molecules in the positive direction. The distortion energies associated with this mode are generally larger than those for the previous modes in which only one molecule is rotated, not surprising in light of the greater misalignment of the central proton and lone pairs caused by this dual rotation. The principal electrostatic effect in $(O_2H_5)^+$ is a destabilizing rotation of the negative end of the OH_2 dipole away from the OH_3^+ unit; similarly, the positive end of the OH_2 dipole is rotated away from the OH^- unit in $(O_2H_3)^-$. Hence, the distortion energies of the cation and anion are not very different from one another for the (40,40) configuration. It is interesting that the anion distortion energies of the (40,0) and (40,40) configurations are quite similar (13.2 and 12.7). In both of these configurations the left-hand OH_2 has been rotated by 40°. If the right-hand molecule is also rotated, its dipole is turned unfavorably from the OH_2 dipole but a stabilizing effect is realized by the better alignment of the central proton and the lone pair. These two competing effects nearly cancel one another leading to approximately equal distortion energies.

The symmetry of the $(O_2H_5)^+$ system leads to identical distortion energies for the (40,40) and (-40,-40) structures. However, these two configurations are quite distinct for $(O_2H_3)^-$ where the clockwise rotation of the OH_2 molecule in the latter mode points the positive end of its dipole more toward OH^-; a second stabilization arises from the rotation of the negative end of the OH^- dipole toward the OH_2 dipole. The net effect is a rather small distortion energy for the (-40,-40) configuration of the anion. The last mode in Table III is associated with the highest distortion energies of all since the central proton and lone pair are rotated away from one another in opposite directions leading to a large misalignment. In both cases, the charge–dipole interaction is a destabilizing one for this configuration. The smaller distortion energy in the anion system may be due to the presence of the out-of-plane lone pairs which can interact with the central proton.

As observed here and previously, the energy barrier to proton transfer is almost always raised as a result of angular distortions of the H bond. This fact may be explained on the same basis as barrier increase with H-bond stretching: in either case, the H bond is weakened and the lone pairs of the proton-accepting and -donating molecules are separated from one another. Therefore, at the approximate midpoint of its transfer the proton must pass through a region of diminished electron density as compared to the case of an undistorted bond. The weaker bonding of the proton and associated destabilization result in the higher transfer barrier. The increase in energy resulting from distortion of the H bond may be clearly seen in the last two columns of Table III. For both $(O_2H_5)^+$ and $(O_2H_3)^-$, rotation of a single lone pair away from the central proton produces a sizable increase in energy (15 kcal/mol for the cation and 10 for the anion). Comparison of the third and fourth with the first and second rows demonstrates that a greater distortion energy arises from rotation of the lone pairs of both molecules than just a single one. Finally, rotation of both lone pairs in *opposite* directions (the last row of the table) leads to an even greater separation of the donor and acceptor lone pairs and correspondingly larger increase in distortion energy.

While the distortion energies of the starting-point configurations of $(O_2H_5)^+$ and $(O_2H_3)^-$ are generally of comparable magnitude, the same is not true for the midpoints where the distortion energies of the cation are uniformly higher than those of the anion. It is for this reason that the increases in barrier height arising from angular distortions are generally greater for $(O_2H_5)^+$. Since the

Table IV. Proton Transfer Barriers (kcal/mol) for H Bonds Involving Angular Distortions (R(OO) = 2.55 Å)

mode	(α_a,α_b), deg	$(O_2H_3)^-$	$(O_2H_5)^+$	$(CH_3OH)_2H^+$
	(0,0)	1.5	1.4	1.9
1	(20,0)	0.9	1.8	2.4
	(40,0)	0.0	5.2	5.6
2	(0,−20)	3.1	1.8	2.7
	(0,−40)	7.0	5.2	8.5
3	(20,20)	1.4	2.7	3.5
	(40,40)	2.2	8.7	9.4
4	(−20,−20)	3.4	2.7	3.5
	(−40,−40)	8.3	8.7	9.4
5	(20,−20)	2.1	2.8	3.2
	(40,−40)	3.0	14.6	14.7

distortion energies of the midpoints are sensitive to separations between donor and acceptor lone pairs, the relative sizes and shapes of the lone pairs in the two systems may play an important role. To address this issue, the electron densities of OH_2 and OH^- were calculated at the 4-31G level and the data examined in the region of the relevant lone pairs. The "lone-pair direction" was defined in each case as leading from the O^b nucleus in Figure 1 along the dashed line representing the H bond. In general the OH^- lone pairs are slightly longer; isodensity contours on this anion extend about 0.01 to 0.03 Å further from the O nucleus than for OH_2. The shapes of the lone pairs are quite similar with both decreasing as one progresses off the direction of the dashed line in the plane of Figure 1. This decrease is slightly less pronounced in the case of OH^- where the out-of-plane lone pairs may make some contribution to the total density.

We illustrate the effects of electrostatics upon the distortion energies of the midpoint configurations by way of Figure 7, parts c and d. The picture is somewhat oversimplified in that a full positive charge is assigned to the central proton but the arguments below would be unchanged with use of some partial charge instead. As before, uncircled + and − symbols are used to indicate the directions of the OH_2 and OH^- dipole moments. (The negative charge of OH^- has not been included in Figure 7d as it is not relevant to the discussion.) The interaction between the positively charged central proton and the negative ends of the two OH_2 dipoles is a very favorable one in the undistorted configuration in Figure 7c. The large distortion energies in the penultimate column of Table III are therefore not surprising as each type of mode leads to a rotation of one or more dipole away from the central proton. On the other hand, the negative ends of the dipoles of OH^- in Figure 7d do not point directly toward the central proton. The first two modes involve a rotation of the negative end of the dipole of one OH^- unit or the other toward the proton and the distortion energy is hence smaller than in the case of Figure 7c. In the third and fourth modes, one OH^- dipole rotates toward the proton and the other away, again a smaller effect than if both rotate away as in the case of $(O_2H_5)^+$. Both hydroxide dipoles rotate toward the H^+ in the last mode, and the distortion energy is therefore dramatically smaller than that for the cation.

An alternative means of interpreting the data arises if one accepts the notion that all three lone pairs of OH^- make available electron density which may be used for bonding to the central proton. Rotations of each OH^- unit which bring the negative end of its dipole toward the proton do not severely diminish the electron density due to the presence of the out-of-plane lone pairs and the distortion energy is correspondingly small. Analogous rotations of OH_2, on the other hand, produce a dramatic drop in available electron density since both lone pairs are rotated away from the proton.

The effects of angular distortion upon proton transfer energetics were also examined in the $(CH_3OH)_2H^+$ system. The computed barriers are presented in Table IV along with analogous data for $(O_2H_5)^+$ and $(O_2H_3)^-$ for purposes of comparison. The results indicate that despite generally higher barriers for $(CH_3OH)_2H^+$ than for $(O_2H_5)^+$, these two systems follow very similar trends. Both show their most dramatic increase for mode 5 where the lone pairs of the two molecules are rotated in opposite directions and a much less severe rise for the first two modes in which only one molecule is rotated. Intermediate between these two cases is the mode consisting of rotation of both molecules in the same direction (modes 3 and 4). Table IV also points out again the very different behavior of the anionic system with respect to angular distortions.

Conclusions

In the case of angularly undistorted H bonds, the proton transfer barriers in the three systems considered here are generally similar, all increasing as the H bond is lengthened. Over the range considered, with H bonds up to 2.95 Å in length, the proton transfer barriers in $(O_2H_5)^+$ and $(O_2H_3)^-$ are nearly identical while those of $(CH_3OH)_2H^+$ are somewhat higher. It is possible to rationalize many of the properties of the proton transfer energetics in terms of simple addition of the proton dissociation potentials of the molecules involved in the transfer. The higher transfer barriers in the methanol dimer may be explained on the basis of the somewhat shorter equilibrium OH bond length in $CH_3OH_2^+$ than in OH_3^+ as the proton is required to move further to reach the midpoint of the H bond. The approximately equal transfer barriers in the anionic system result from partial cancellation between two opposing influences. The protonated OH^- anion contains a shorter OH bond which would lead to a higher barrier, but the longer lone pairs of OH^- produce an opposite effect.

Angular deformations of the H bond generally lead to increases in the transfer barrier for any given bond length. The barrier increases are quite similar in the cationic $(O_2H_5)^+$ and $(CH_3OH)_2H^+$ systems and obey the simple rule that greater misalignments of the lone pairs of the proton-donating and -accepting molecules lead to higher barriers. The behavior of the anionic $(O_2H_3)^-$ is quite different, but the various effects of angular distortions upon the proton transfer energetics in all three systems may be simply explained in terms of electrostatic arguments, making use of the charges and dipoles of the subunits concerned.

A good deal of additional information may be extracted from the alterations in electronic structure caused by the motion of the central proton. An overall shift of electron density occurs in the direction opposite to the motion of the proton. The proton-donating methanol is able to pick up more density than the other subunits due to the presence of the methyl group which acts as an effective sink for the additional charge. This density is shifted into the methyl group via polarizations of the appropriate CO and CH bonds. The methyl group on the proton-accepting molecule serves an analogous function as a source of density for the remainder of the system. In fact, enough charge is shifted from this methyl group to the proton-accepting oxygen that the latter atom *gains* density as a result of the proton transfer, in marked contrast to the losses sustained by the same atom of the other two systems. The polarizable character of the OH^- anion allows a significantly larger amount of density to be extracted from it than from the proton-accepting OH_2 or CH_3OH groups. In contrast to the cationic systems, the proton-accepting oxygen atom of OH^- loses a great deal of its density from a region centered along the H-bond axis and on the opposite side of the O nucleus from the approaching proton. The patterns of density change in the regions of the oxygen lone pairs are quite similar in all three systems, leading to the conclusion that these patterns are characteristic of O atoms in general.

Acknowledgment. This work was financially supported by the National Institutes of Health (GM29391 and AM01059) and by the Research Corporation. A grant of computer time was provided by the SIU Computing Center.

Registry No. Hydroxide, 14280-30-9; water, 7732-18-5; methanol, 67-56-1; oxonium, 13968-08-6; protonated methanol, 17836-08-7.